# Biaxiality-driven twist-bend to splay-bend nematic phase transition induced by an electric field

Claire Meyer, Christophe Blanc, Geoffrey R. Luckhurst, Patrick Davidson, Ivan Dozov

MATERIALS SCIENCE

# Biaxiality-driven twist-bend to splay-bend nematic phase transition induced by an electric field

Claire Meyer[1], Christophe Blanc[2], Geoffrey R. Luckhurst[3], Patrick Davidson[4], Ivan Dozov[1,2,4]*



**Although the existence of the twist-bend ($N_{TB}$) and splay-bend ($N_{SB}$) nematic phases was predicted long ago, only the former has as yet been observed experimentally, whereas the latter remains elusive. This is especially disappointing because the $N_{SB}$ nematic is promising for applications in electro-optic devices. By applying an electric field to a planar cell filled with the compound CB7CB, we have found an $N_{TB}$-$N_{SB}$ phase transition using birefringence measurements. This field-induced transition to the biaxial $N_{SB}$ occurred, although the field was applied along the symmetry axis of the macroscopically uniaxial $N_{TB}$. Therefore, this transition is a counterintuitive example of breaking of the macroscopic uniaxial symmetry. We show by theoretical modeling that the transition cannot be explained without considering explicitly the biaxiality of both phases at the microscopic scale. This strongly suggests that molecular biaxiality should be a key factor favoring the stability of the $N_{SB}$ phase.**

## INTRODUCTION

The nematic (N) phase is the most common thermotropic liquid crystalline state. In the usual nematic, the rod-like achiral molecules orient on average parallel to a common direction, **n**, called the "director." The nematic long-range orientational order is described by a uniaxial second-rank tensor, $Q_{ik} = (S/2)(3n_i n_k - \delta_{ik})$, with the scalar order parameter, $S = \langle 3\cos^2\beta - 1\rangle/2$, where β is the angle between the molecular long axis and the director, and the brackets denote a statistical average (*1*). Any deviation of *S* from its equilibrium value, $S_0(T)$, costs a huge energy. In contrast, the nematic energy is unaffected by a uniform rotation of the director and only the director distortions, imposed by the boundary conditions or by external fields, cost some elastic energy (*2*)

$$f_{el} = \frac{1}{2}\{K_{11}\,\mathbf{s}^2 + K_{22}\,t^2 + K_{33}\,\mathbf{b}^2\} \quad (1)$$

where the vectors $\mathbf{s} = \mathbf{n}(\nabla \cdot \mathbf{n})$, $\mathbf{b} = \mathbf{n} \times (\nabla \times \mathbf{n})$, and the pseudoscalar $t = -\,\mathbf{n} \cdot (\nabla \times \mathbf{n})$ describe the main distortion modes splay, bend, and twist, respectively. At equilibrium, the N phase is uniform, with $\nabla\mathbf{n} = 0$. However, the chiral nematic (N*) phase, or cholesteric, formed by chiral molecules, is spontaneously twisted, with **n** following a right-angle helix of pitch, $p^*$, usually larger than a few hundred nanometers. Then, the twist term in Eq. 1 becomes $K_{22}\,(t - t_0)^2$, where $t_0 = \pm\,1/p^*$ is the spontaneous twist induced by the molecular chirality.

Different nematic phases are expected when the mesogenic molecules are less symmetric. For example, a biaxial nematic has been predicted (*3*) when the molecular structure and interactions are strongly biaxial. However, although it was reported in lyotropic systems, it is most elusive in thermotropic ones. For strongly bent mesogenic molecules, studies based on different physical mechanisms predicted the existence of a nematic phase with spontaneous bend distortion of the director (*4*, *5*). However, unlike twist, a pure bend distortion cannot fill space without introducing energy-expensive defects. Mixed-distortion modes (*4*, *5*), either twist + bend or splay + bend, avoid this constraint and lead to two modulated nematic (MN) phases, the twist-bend ($N_{TB}$) and splay-bend ($N_{SB}$) phases, respectively. In the $N_{TB}$ phase, the director is arranged on a heliconical structure (Fig. 1), $\mathbf{n} = (\sin\theta\sin\varphi, \sin\theta\cos\varphi, \cos\theta)$, where $0 < \theta < \pi/2$ is the heliconical tilt angle (i.e., the angle between **n** and the helix axis, **h**), $\varphi = qZ$ is the phase of the precession of **n** around **h**, and $q = \pm\,2\pi/p$ is the wave number of the director "wave" of wavelength *p*. The sign of *q* describes the handedness of the helix. Even with achiral molecules, the $N_{TB}$ phase is chiral, with broken chiral symmetry (*5*) and doubly degenerate chirality, and it consists of right and left monochiral domains. The occurrence of the $N_{TB}$ phase then appears as an especially interesting case of spontaneous chiral symmetry breaking.

In contrast, the $N_{SB}$ phase is achiral when the molecules are achiral. It can be regarded, approximately, as a sine-wave oscillation of the director (Fig. 1) $\mathbf{n} = (0, \sin(\theta_0\sin\varphi), \cos(\theta_0\sin\varphi))$, where $\theta_0 < \pi/2$ is the oscillation amplitude and $\varphi \approx qZ$ is its phase. Therefore, the $N_{SB}$ phase is described by a linearly polarized wave of director distortion. By symmetry, all the orientations of the polarization are equivalent and correspond to the same continuously degenerate ground state. Note that this phase should not be confused with the "splay nematic" phase that was recently discovered with strongly polar calamitic mesogens (*6*–*8*). The splay nematic phase is characterized by a spontaneous splay distortion instead of the spontaneous bend distortion that induces the $N_{TB}$ and $N_{SB}$ phases.

The three different nematic phases (N, $N_{TB}$, and $N_{SB}$) expected for bent-shaped mesogenic molecules have different macroscopic symmetries. For achiral molecules (considered here), the N phase is uniaxial and achiral. The $N_{TB}$ phase, however, has broken chiral symmetry and is locally biaxial. Because of the strong spontaneous bend distortion, the uniaxial symmetry around **n** is broken. However, because of the precession of **n** around **h**, the $N_{TB}$ phase remains macroscopically uniaxial (at scales much larger than the pitch *p*). The $N_{SB}$ phase is achiral, like the N phase, but is locally biaxial, like the $N_{TB}$ phase. Moreover, the $N_{SB}$ phase is biaxial even at a macroscopic scale because the plane in which **n** oscillates is unique (Fig. 1).

In both MN phases, the bend is spontaneous, but the splay and twist cost some elastic energy. Therefore, the relative stability of the

[1]Physique des Systèmes Complexes, Université de Picardie Jules Verne, 80039 Amiens, France. [2]Laboratoire Charles Coulomb, UMR 5221, CNRS-Université de Montpellier, 34095 Montpellier, France. [3]School of Chemistry, Faculty of Engineering and Physical Sciences, University of Southampton, Highfield, Southampton SO17 1BJ, UK. [4]Laboratoire de Physique des Solides, CNRS, Univ. Paris-Sud, Université Paris-Saclay, 91405 Orsay Cedex, France.
*Corresponding author. Email: ivan.dozov@u-psud.fr

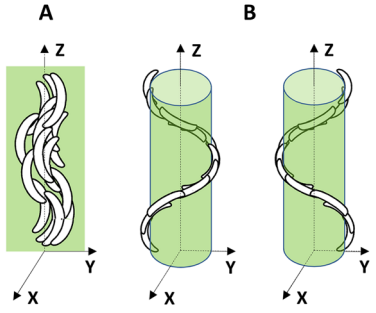


**Fig. 1. Schematic views of the structure of the modulated nematic phases formed by achiral bent-shaped molecules.** (**A**) In the splay-bend nematic phase, the director oscillates in a plane, chosen here to be the **YZ** plane of the laboratory frame **XYZ**. (**B**) In the twist-bend nematic phase, the director is arranged on a conical helix with doubly degenerate chirality. The helix axis, **h**, is parallel to the **Z** axis of the laboratory frame.

two phases depends on $K_{11}/K_{22}$, and the stable phase is $N_{TB}$ for $K_{11}/K_{22} \geq 2$ and $N_{SB}$ otherwise (*5*, *9*).

Starting from 2008, several groups reported a second, low-temperature, nematic phase, called $N_X$ (originally, the mnemonic $N_X$ was used for a nematic phase with an unknown structure; subsequently, it has been taken to denote the $N_{TB}$ phase) for bent-shaped mesogens, which presented some of the properties predicted for modulated nematics (*10*–*13*). Then, Cestari *et al.* (*14*) demonstrated that the $N_X$ phase is the predicted $N_{TB}$ phase. Later studies confirmed this assignment (*15*) and showed either indirectly (*16*, *17*) or in direct FFTEM (freeze-fracture transmission electron microscopy) (*18*, *19*) and resonance x-ray scattering (*20*) experiments that $p$ is extremely small ($p < 10$ nm). Most of the defining properties of the $N_{TB}$ phase were also confirmed: the temperature-dependent conical angle (*16*, *18*, *19*, *21*), the chiral symmetry breaking (*14*, *22*), the existence of large monochiral domains (*16*, *18*, *21*), and the strong pretransitional decrease of $K_{33}$ in the nematic phase (*14*, *23*–*25*).

Further synthetic work (*26*–*29*) and experimental studies demonstrated that the $N_{TB}$ phase is quite widespread for bent-shaped dimers. In stark contrast, the $N_{SB}$ phase has yet to be observed, in the absence of an external constraint, for any compound. The elusiveness of the $N_{SB}$ phase indicates that the low $K_{11}/K_{22}$ ratio is only a qualitative criterion for its thermodynamic stability. However, an $N_{TB}$ to $N_{SB}$ transition could be induced by the topological constraint of a defect wall between two monochiral $N_{TB}$ domains with opposite chiralities (*21*).

Strong fields applied to the $N_{TB}$ phase may also induce phase transitions. Under a magnetic field of 25 T, the bent-shaped CB7CB [1″,7″-*bis*(4-cyanobiphenyl-4′-yl) heptane] dimer showed a weak decrease ($\Delta T_{NTB-N} = 0.7$ K) of the N-$N_{TB}$ transition temperature (*30*). A similar effect is also expected (*31*, *32*) when a strong electric field, **E**, is applied parallel to **h** in the $N_{TB}$ phase of a compound with positive dielectric anisotropy, $\Delta\varepsilon > 0$. So far, the estimates of the field strength required for a measurable transition shift range from a few (*31*, *33*) to 100 V/μm (*32*). For $\Delta\varepsilon < 0$ and/or $\mathbf{E} \perp \mathbf{h}$, the uniaxial symmetry of the $N_{TB}$ phase is broken and the $N_{TB}$ cone becomes elliptical, leading eventually, as expected, to an $N_{TB}$ to $N_{SB}$ transition (*31*–*33*). Strong planar surface anchoring may also act as a field, breaking the uniaxial macroscopic symmetry of the $N_{TB}$ phase, leading to an elliptical $N_{TB}$ cone (*34*) and, in the case of extremely strong anchoring, to a surface-induced transition to the $N_{SB}$ phase (*35*).

Here, we report on a field-induced $N_{TB}$-$N_{SB}$ phase transition, of CB7CB, with $\Delta\varepsilon > 0$, in a quite different geometry. In a cell with planar alignment of the helix axis, **h**, we apply a strong, in-plane electric field, $\mathbf{E} \parallel \mathbf{h}$. At $E = 0$, we observe the usual N-$N_{TB}$ phase transition at temperature $T_{NTB-N}$. Under a field, we observe a small decrease of $T_{NTB-N}$, as expected. However, the birefringence $\Delta n(T)$ measured in the low-temperature phase differs drastically from those of both the N and $N_{TB}$ phases. Instead, it is similar to that measured (*21*) in a defect wall with an $N_{SB}$ structure. This unexpected result indicates a symmetry-breaking transition from the macroscopically uniaxial $N_{TB}$ phase to a field-induced macroscopically biaxial $N_{SB}$ phase. This transition then appears as a clear example of uniaxial symmetry breaking. Using a simple model, we show that the field-induced transition is due to the biaxial order at the microscopic scale in both $N_{TB}$ and $N_{SB}$ phases.

## RESULTS

### Polarized optical microscopy

The field-induced phase transition is observed in a planar cell filled with the dimer CB7CB (see Fig. 2 and Materials and Methods for details) with a field applied parallel to **n** (in the nematic phase) or to **h** (in the $N_{TB}$ phase). In the nematic phase ($T = 103.4$°C), without a field (Fig. 3A), the alignment of the sample is excellent, in the active region (AR) between the electrodes and above the electrodes, with **n** parallel to the substrates and to the rubbing direction **r**. Under the electric field (Fig. 3B, $E = 8$ V/μm), the director orientation remains the same in the AR, except close to the electrode edges. The field distribution in the cell (Fig. 2B) is highly uniform, with $\mathbf{E} \parallel \mathbf{r}$, in the middle of the AR. Moreover, no birefringence variation is observed under the field, which indicates that $S$ is not affected by the field. In contrast, the birefringence varies rapidly above the electrode edges because **n** lies parallel to the tilted field there (Fig. 2B).

Upon slow cooling at $E = 0$, the nematic-isotropic (N-I) transition occurs at $T_{N-I} = 115.8 \pm 0.2$°C, in reasonable agreement with previous studies (*14*, *16*, *29*). A small biphasic region of 0.4°C was measured at the center of the field of view, and we also observed a weak temperature variation, of about 0.2°C, along the AR. The texture of the N phase remains uniform, with $\mathbf{n} \parallel \mathbf{r}$ (fig. S1). The N-$N_{TB}$ phase transition occurs at $T_{NTB-N} = 103.1 \pm 0.1$°C by progressive growth of domains (fig. S1, A to C), and after the last nematic domains have disappeared, the texture is again approximately uniform (fig. S1D), with the $N_{TB}$ optic axis $\mathbf{N} \parallel \mathbf{r}$. Upon further cooling, the typical textural instabilities (*14*) of the $N_{TB}$ phase appear (fig. S1, C to J): stripe texture, rope texture, and finally focal conic domains. These textural variations are essentially reversible, albeit with some hysteresis far away from $T_{NTB-N}$ (fig. S1, K and L).

Upon slow cooling under the field (8 V/μm), the N-I transition occurs at $T_{N-I} = 115.5 \pm 0.3$°C, revealing a moderate heating by the field in the AR. Throughout the temperature range of the N phase, the texture remains as in Fig. 3B but with the interference color varying with the temperature. The N-$N_{TB}$ transition is first observed above the electrodes, at $T_{NTB-N} = 103.1$°C. At 103.0°C, this whole area is in the $N_{TB}$ phase (Fig. 3, C and D), with homeotropic alignment close to the electrode edges because of the strongly tilted field there. However, in the AR, the sample still remains in the nematic phase, suggesting a small decrease of $T_{NTB-N}$ under the field, by $\Delta T_{NTB-N} = 0.1$° to 0.2°C, as expected by analogy with the magnetic field case (*30*). This shift of $T_{NTB-N}$ might also be due to the Joule

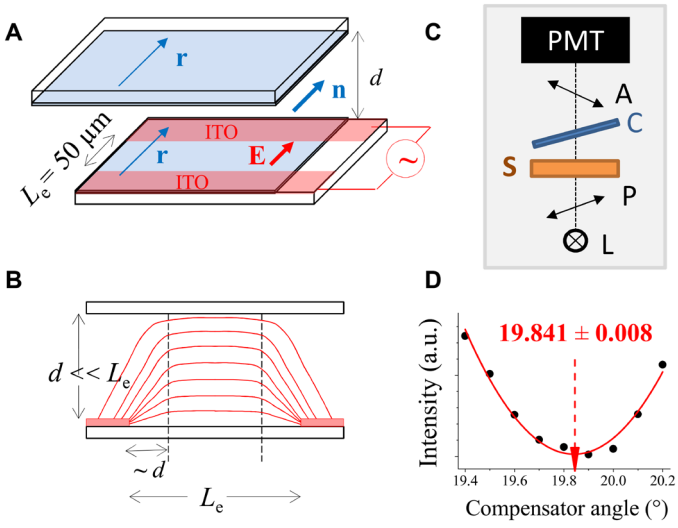


**Fig. 2. Cell and setup for the electro-optical measurements.** (**A**) The two plates of the cell are covered with a PVA layer (shaded in blue), rubbed along the direction **r**; the in-plane field **E** ∥ **r** is applied across the two ITO electrodes placed on the bottom plate (shaded in red). (**B**) Schematic view of the electric field lines in a cross section of the cell. For clarity, the vertical scale is expanded. Close to the electrodes, the field direction and strength vary rapidly because of the edge effects; farther from the ITO stripes, the field is homogeneous and parallel to the substrates and to the rubbing direction **r**. (**C**) Setup for the measurement of the phase shift of the light transmitted by the cell. (**D**) Typical curve of the transmitted intensity as a function of the tilt angle 2*i* of the Berek compensator; the fit of the data points with a parabola improves significantly the precision of the measurement. The red arrow shows the fitted value of the minimum of the parabola. a.u., arbitrary units.

heating of CB7CB by the electric field, estimated to ~0.1°C in our in-plane field geometry.

Upon further slow cooling, the region over the electrodes remains in the $N_{TB}$ phase, and its texture evolves through defect propagation from homeotropic to smectic-like focal conic defects (Fig. 3, E to L). Meanwhile, in the AR, a phase transition to another nematic-like phase occurs at 102.9°C. Because both phases are well aligned by the field and have almost the same birefringence, the transition is hardly visible under crossed polarizers (Fig. 3E). However, with a Berek compensator in the optical path (Fig. 3F), the sharp limit between the two phases is easily detected because they differ slightly in their birefringence. Because of a small in-plane temperature gradient across the cell, the new phase first appears in the cooler left-hand bottom corner of the sample and spreads slowly toward the hotter (by 0.1°C) right-hand top corner. The phase-separation line has a parabolic meniscus-like shape consistent with a field-induced shift of the transition temperature as $\Delta T_{NTB-N}$ increases with increasing field strength (the field being stronger close to the electrode edges).

At first glance, the textural observations of the low-temperature phase are compatible with its expected $N_{TB}$ nature. However, detailed measurements (see the next section) revealed that its birefringence is drastically different from those of both the nematic and the $N_{TB}$ phases, indicating the distinct nature of the field-induced phase. Therefore, for the time being, we will label this yet to be identified, low-temperature, nematic phase as "$N_Y$" (we avoid the ambiguous notation $N_X$ because it was already used in a different context).

Upon further cooling in the field, the AR remains in the $N_Y$ phase, but its texture progressively evolves. Close to the $N_Y$-N transition, the texture remains perfectly uniform, with **N** ∥ **r** (Fig. 3, G and H), which allowed us to measure precisely the birefringence. When the

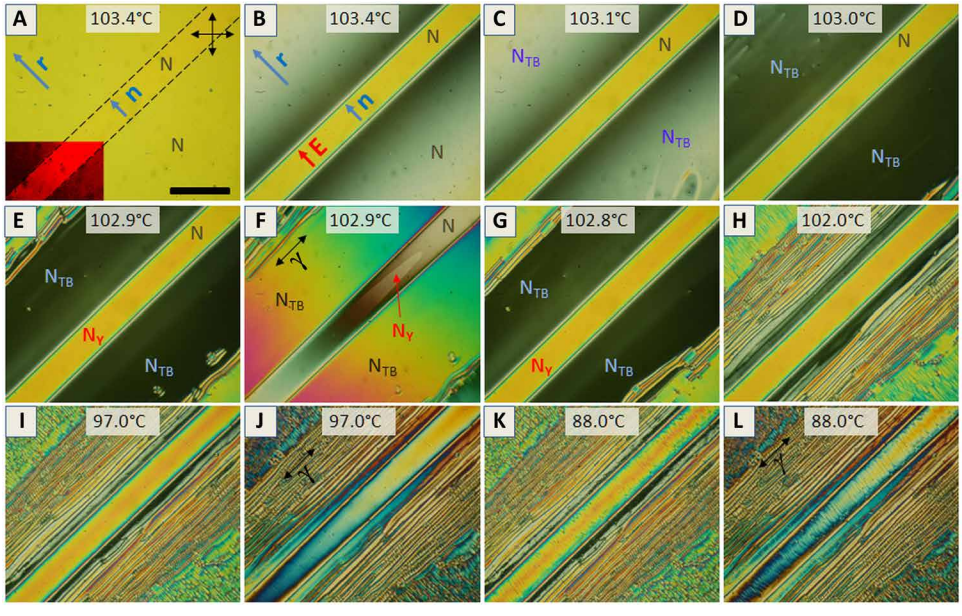


**Fig. 3. Textures and phase transitions at varying field and temperature.** Scale bar, 100 μm. In (**A**) the field is switched off and in (**B** to **L**) a square waveform field is applied, $E = 8$ V/mm,10 kHz. (A) In the N phase, at $E = 0$, the director **n** is parallel to the rubbing direction **r**. The dashed lines delimit the AR between the electrodes. In the corner, the contrast is saturated to show the slightly larger birefringence in the AR. (B) Subject to the field, **n** is parallel to **r** in the AR, but is tilted outside of it. (C and D) On cooling, the $N_{TB}$ phase first appears outside of the AR, meaning that the N-$N_{TB}$ transition is shifted. (E and F) The N-$N_Y$ phase transition takes place in the AR. To reveal the small birefringence jump at the transition, (F) was recorded with a Berek compensator (γ shows its slow axis). (G to L) Upon further cooling, no other phase transition occurs but, in the region subject to the field, the texture becomes progressively less homogeneous: First very weak, stripe instabilities appear (G and H), then they become more contrasted (I and J), and finally the electrode edges are decorated by focal conics (K and L). For (J) and (L), the Berek compensator was introduced again.

temperature is decreased further, some stripes appear in the AR (Fig. 3, I and J), with a contrast much weaker than in the absence of the field (for comparison, see fig. S1). Farther from the $N_Y$-N transition, the stripes become more marked but are still hardly visible between the crossed polarizers without a compensator. In this temperature range, the birefringence measurements are still possible with a reasonable precision. Upon further cooling, these stripes have greater contrast (Fig. 3, K and L) and some focal conic domains appear close to the electrode edges, preventing any precise birefringence measurements.

Close to $T_{NY-N}$, the texture changes induced by temperature variations at constant field are reversible, with little or no hysteresis. Moreover, at a fixed temperature in this range, a fast birefringence response is observed upon variation of the field strength (fig. S2). Both observations suggest that the $N_Y$ phase is not a smectic but a modulated nematic phase despite its smectic-like textures at lower temperatures. Such textures are expected not only from the $N_{TB}$ phase but also from other MN phases (such as the $N_{SB}$ phase), because of their pseudo-layered structures (*14*, *32*, *36*).

Further from the transition, the response of the texture to a variation in temperature shows more hysteresis (about 2° to 3°C at 88°C) and the response to a variation in field strength completely disappears. Switching the field on and off at 88°C has practically no effect on the texture, which is apparently "frozen" because of the stiffening of the pseudo-layered structure, the entanglement of the defects, and the smectic- and $N_{TB}$-like increase of the viscosity.

To summarize the influence of temperature and electric field intensity, because the birefringence values measured under field are not influenced by the thermal history, the existence of the field-induced $N_{SB}$ phase does not depend on the thermodynamic path used experimentally.

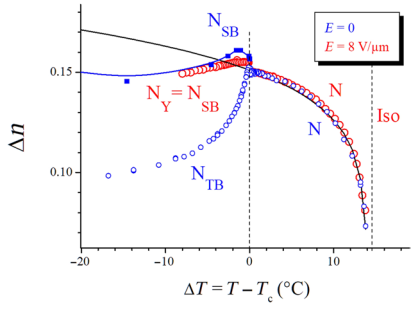


**Fig. 4. Birefringence of CB7CB measured as a function of temperature in different phases.** The open red symbols show the data measured in the present study subject to the field $E = 8$ V/μm in the nematic and $N_Y$ (now identified as the $N_{SB}$ phase) phases. The blue symbols show the data from (*21*) measured without applied field in the N and $N_{TB}$ phases of the same mesogen in a thin (1.6-μm) cell. The open symbols show the birefringence measured in the N phase or in large monochiral, uniform domains of the $N_{TB}$ phase. The full squares show the birefringence data measured in the defect wall with an $N_{SB}$ structure, which separates these monochiral domains (the line connecting them is a guide to the eye and does not have any physical meaning). The good agreement of those $N_{SB}$ data with our present results obtained under a field identifies the $N_Y$ phase with the $N_{SB}$ phase. The continuous black line shows the birefringence expected in the nematic phase (obtained by extrapolation of the Haller function). Its temperature dependence is different from that of the $N_Y$ phase, which confirms that the field-induced phase is not the usual uniform nematic but a distinct state. It is also of interest that, in the field experiment, the birefringence exhibits a clear jump at the $N_{SB}$-N transition, which would be consistent with the first-order nature of the transition. Subsequently, the birefringence passes through a weak maximum before decreasing essentially in a linear manner in keeping with that in the defect walls.

## Birefringence of the field-induced nematic phase

Qualitatively, the behavior of the $N_Y$ phase is that expected for the $N_{TB}$ phase subject to a strong field, **E**, oriented parallel to the optic axis **N** (*31*, *32*). Macroscopically, the torque applied by the field to the local $N_{TB}$ director **n** is elastically transmitted to **N**, which favors the uniform alignment of **h** parallel to **E**. Close to $T_{NTB-N}$, the torque is large enough to ensure uniform alignment of **N**. At lower temperatures, the torque is too weak to affect the stiffer macroscopic elasticity of the $N_{TB}$-phase and the intrinsic textural instabilities of the phase reappear (Fig. 3, I to L).

Apart from the macroscopic alignment, sufficiently strong fields could modify the microscopic heliconical structure by decreasing the cone angle, leading eventually to a second-order $N_{TB}$-N transition (*31*, *32*). Experimentally, this should result in a tiny, field-dependent decrease of the $N_{TB}$-N transition temperature, as observed here. However, the detailed test of this hypothesis is difficult in the electric field case because of a possible local heating of the sample. On the contrary, when the texture is uniformly aligned, the precise measurement of the birefringence, $\Delta n$, provides the field dependence of the conical angle and, more generally, information on the microscopic structure of the phase (*21*). In the AR, where $\Delta n$ is measured, the texture is perfectly uniform in the nematic phase, with or without field. However, it is only sufficiently uniform over ~0.2°C below the transition in the $N_{TB}$ phase (without field), and over ~5° to 8°C below the transition in the $N_Y$-phase (for fields between 4 and 20 V/μm).

The temperature dependence of $\Delta n$ was measured under the field in the N and $N_Y$ phases (Fig. 4), and a few data points were also measured in the N phase at $E = 0$. These points cannot be distinguished from those measured under the field, which confirm that the field is too weak to affect *S*. For comparison, Fig. 4 also shows previous birefringence measurements in the N and $N_{TB}$ phases of CB7CB at $E = 0$ in a very thin (1.6 μm) cell (*21*). This cell displayed, in the $N_{TB}$ phase, large and perfectly uniform monochiral domains, with right-handed (R) and left-handed (L) chirality. The birefringence is the same in the R and L domains, and it is drastically different from the Haller extrapolation of $\Delta n$ from the nematic state, because of the increase of the conical angle of the $N_{TB}$ helix (*16*) from ~10° to ~35° upon decreasing temperature (*21*). A completely different birefringence has been measured in the defect walls separating the R and L domains (*21*). This revealed that the structure in the walls of the modulated nematic is $N_{SB}$ instead of $N_{TB}$ because of the topological incompatibility of the helices of opposite chiralities. Both N and $N_{SB}$ "cores" of the defect wall would satisfy the topological constraint, but the $N_{SB}$ structure costs less energy (*21*) than the nematic one because it keeps the spontaneous bend distortion (at least partially).

Throughout the nematic phase, the birefringence curves, measured with or without the field, are almost superimposed (Fig. 4). In stark contrast, the $\Delta n$ data measured in the $N_Y$ phase under the field are completely different from the previous zero-field $N_{TB}$ data (*21*) but lie very close to the data previously measured in the $N_{SB}$ defect wall. This provides clear evidence that a large enough field **E** parallel to **N** induces an $N_{TB}$-$N_{SB}$ transition, instead of the $N_{TB}$-N transition expected theoretically. Therefore, the $N_Y$ phase is a field-induced $N_{SB}$ phase.

## Theoretical model

To understand the unexpected field-induced $N_{TB}$-$N_{SB}$ transition, we compare the energies of the N, $N_{TB}$, and $N_{SB}$ phases as a function of the temperature and the applied field. In the absence of a field, two models have been proposed to obtain the N-$N_{TB}$-$N_{SB}$ phase diagram. The first that we will follow here is the "elastic-instability" model (*5*). It considers the MN phases of bent-shaped molecules as usual uniaxial nematics with a negative $K_{33}$. The elastic energy is given by $f_{el} = f_{II} + f_{IV}$, where $f_{II}$, the Frank elastic energy (Eq. 1), is quadratic in **n** gradients, whereas $f_{IV}$, which is quartic in **n** gradients, is required to bind the energy from below when $K_{33} < 0$. As the bend elastic constant changes sign at the N-$N_{TB}$ transition, it is expected that close to the transition temperature, $T_{NTB\text{-}N}$, $K_{33}$ depends linearly on the temperature: $K_{33}(T) = a(T - T^*)$, and the weak temperature dependence of all the other elastic constants can be neglected (*23*, *25*). Here, $T^*$ is the temperature of the second-order N-$N_{TB}$ phase transition predicted by the model. (Because the N-$N_{TB}$ transition for CB7CB is weakly first order, as explained in Discussion, $T^*$ is slightly different from the experimentally observed transition temperature, $T_{NTB\text{-}N}$). The experimental results for $K_{33}(T)$ in the nematic phase of CB7CB (see fig. S3) confirm the predicted linear dependence and provide the slope, $a = 0.066$ pN/K.

To model the electric field effects in the N and MN phases, we also need to couple the nematic order parameter tensor, **Q**, with the electric field. Only the quadratic (in **E**) dielectric coupling is important here because the polar flexoelectric contribution to the total energy integrates to zero (*16*, *32*). Therefore, the electric contribution to the free energy density is $\Delta f(E) = -\varepsilon_0 \mathbf{E} \cdot \boldsymbol{\varepsilon} \cdot \mathbf{E}/2$, where $\boldsymbol{\varepsilon}$ is the dielectric susceptibility tensor. In general, like **Q**, $\boldsymbol{\varepsilon}$ has different symmetry and orientation with respect to **E** in the three considered phases. The average conformation of the bent-shaped dimer only has $C_{2v}$ symmetry (Fig. 5A) and is therefore polar and biaxial. We choose the molecular frame **123** with the **3**-axis parallel to the long molecular axis and the **2**-axis along the $C_2$ axis. The N phase has a higher symmetry, $D_{\infty h}$, and we choose the director-frame **xyz** with the $z$ axis along the $D_\infty$ axis (i.e., along **n**). Then, the orientational order is described by the usual uniaxial tensor, $\mathbf{Q}^u$, which is diagonal in the **xyz** frame. In the MN phases, however, the macroscopic uniaxial symmetry is broken by the strong spontaneous bend, **b**. There is no longer revolution symmetry around **n** and the phases are biaxial and polar (*5*, *9*, *36*, *37*), at least locally, at scales smaller than $p$. Therefore, **Q** is biaxial, $\mathbf{Q} = \mathbf{Q}^b$, and choosing the ***y*** axis parallel to **b** (Fig. 5A), we have in the director frame (*38*)

$$\mathbf{Q}^u = \frac{1}{2}\begin{pmatrix} -S & 0 & 0 \\ 0 & -S & 0 \\ 0 & 0 & 2S \end{pmatrix}; \quad \mathbf{Q}^b = \frac{1}{2}\begin{pmatrix} -S-P & 0 & 0 \\ 0 & -S+P & 0 \\ 0 & 0 & 2S \end{pmatrix} = \mathbf{Q}^u + \frac{1}{2}P\begin{pmatrix} -1 & 0 & 0 \\ 0 & 1 & 0 \\ 0 & 0 & 0 \end{pmatrix} \tag{2}$$

where $S$ is the usual uniaxial scalar order parameter and $P$, the secondary order parameter, describes the biaxiality of the MN phase.

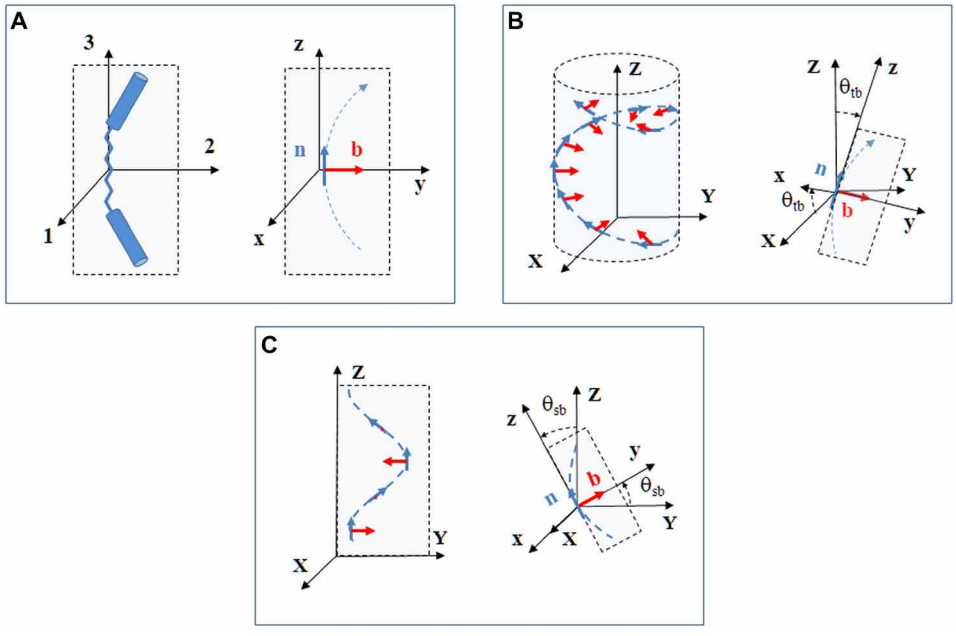


**Fig. 5. Definitions and mutual orientations of the molecular, director, and laboratory frames.** The blue dashed lines show the trajectory of the director **n**. (**A**) The averaged conformer of the dimer is taken to be planar with $C_{2v}$ symmetry. The **2**-axis of the molecular frame **123** is chosen to be along the $C_2$ symmetry axis. The highly polarizable rigid cores of the monomers (shown as cylinders) lie in the **23**-plane. The axis **3** is parallel to the main axis of the conformer, and its average orientation defines the director **n**. The **z** axis of the director frame **xyz** is parallel to **n**. The N phase is uniaxial and the orientation of the **y** axis is arbitrary. In the MN phases, the uniaxial symmetry is broken because of the strong bend of the director, and we choose the **y** axis parallel to the bend vector, $\mathbf{b} = \mathbf{n} \times (\nabla \times \mathbf{n})$. The biphenyl cores of the monomers are oriented preferentially parallel to the local director at their position, resulting in average orientation of the dimer with **3** ∥ **z** and **2** ∥ **y**. As the molecular polarizability, $\boldsymbol{\alpha}$, is due mainly to the biphenyl groups, and because the dielectric tensor, $\varepsilon = \varepsilon^b$, is related to the average of $\boldsymbol{\alpha}$, we expect $\varepsilon^b_{xx} < \varepsilon^b_{yy} < \varepsilon^b_{zz}$ in the MN phases. (**B**) In the $N_{TB}$ phase, the laboratory frame **XYZ** is defined by **Z** parallel to **E** (and to the helix axis **h**) and arbitrary orientation of **Y**. As **y** ∥ **b** and **b** ⊥ **Z**, the **Z** axis lies in the **xz** plane, tilted at a fixed angle $\theta_{tb}$ with respect to **z**. (**C**) In the $N_{SB}$ phase, the **Y** axis is no longer arbitrary and is chosen to lie in the **yz** plane of the director frame. Therefore, the **Z** axis also lies in that plane and is periodic with respect to the **z** axis by a position-dependent angle $\theta_{sb}(Z)$.

In principle, $S$ and $P$ can be calculated using molecular field theory and atomistic modeling (*14*, *39*–*41*). However, close to the N-MN transition, a simple symmetry-based approach gives $P = \beta_2 \mathbf{b}^2 \ll S$ (see Materials and Methods), where $\beta_2$ is a material constant.

The dielectric tensor, diagonal in the director frame, is uniaxial in the N phase

$$\boldsymbol{\varepsilon}^{u} = \begin{pmatrix} \varepsilon^{u}_{xx} & 0 & 0 \\ 0 & \varepsilon^{u}_{yy} & 0 \\ 0 & 0 & \varepsilon^{u}_{zz} \end{pmatrix} = \bar{\varepsilon}\mathbf{I} + \delta\varepsilon^{u}\mathbf{Q}^{u} \quad (3)$$

(with $\varepsilon^{u}_{xx} = \varepsilon^{u}_{yy}$) and it is biaxial in the MN phases

$$\boldsymbol{\varepsilon}^{b} = \begin{pmatrix} \varepsilon^{b}_{xx} & 0 & 0 \\ 0 & \varepsilon^{b}_{yy} & 0 \\ 0 & 0 & \varepsilon^{b}_{zz} \end{pmatrix} = \bar{\varepsilon}\mathbf{I} + \delta\varepsilon^{u}\mathbf{Q}^{u} + \frac{1}{2}\delta\varepsilon^{b} P \begin{pmatrix} -1 & 0 & 0 \\ 0 & 1 & 0 \\ 0 & 0 & 0 \end{pmatrix} \quad (4)$$

where $\mathbf{I}$ is the unit tensor and $\bar{\varepsilon}, \delta\varepsilon^{u}$ and $\delta\varepsilon^{b}$ are material constants (see Materials and Methods). Although $\boldsymbol{\varepsilon}^{b}$ is the same in the two MN phases in this approximation, the dielectric contribution to the energy is different because of the different orientations of the director frame with respect to the field (Fig. 5).

In the absence of the field, the minimized (i.e., ground-state) energy densities of the N, $N_{TB}$, and $N_{SB}$ phases are respectively [see (*5*) and the Supplementary Materials]

$$\bar{f}_N = 0; \quad \bar{f}_{NTB} = \frac{{K_{33}}^3}{54\,K_{22}\,C}; \quad \bar{f}_{NSB} = \frac{{K_{33}}^3}{27\,K_{11}\,C} \quad (5)$$

where $C$ is a fourth-order elastic modulus, and for the $N_{SB}$ case, we used the "harmonic" approximation, $\theta_{sb}(Z) = \theta_0 \sin(q_{sb}Z)$.

In this approximation, the N-$N_{TB}$-$N_{SB}$ phase diagram as a function of the dimensionless ratios $R_3 = K_{33}(T)/K_{22}$, and $R_1 = K_{11}/K_{22}$ is very simple (Fig. 6A). For $R_3 > 0$, i.e., for $T > T^*$, the only solution is the N phase, with $\bar{f}_N = 0$. For $R_3 < 0$, the energies of the modulated phases are negative, resulting in a second-order N-MN transition at the line $R_3 = R_3^c = 0$ (or $T = T^*$). [The predicted transition is second order due to the approximations made in (*5*), but our experiments and more recent theoretical models (*42*) show that the $N_{TB}$-N transition is first order.] The transition line between the two modulated phases occurs at $R_1^c = 2$ and is therefore approximately temperature independent. Similar results were obtained by Shamid *et al.* (*9*) in a flexoelectric model for the N-MN transition. The analytical approximation also gives $R_1^c = 2$, while the exact numerical value, 2.17, is only 8% higher (*9*).

Subject to the field, we expect a field-induced shift, $\Delta R_i^c(E) = R_i^c(E) - R_i^c(0)$, $i = 1$ or 3, of the phase boundary lines. Let us first neglect the biaxiality of the MN phases and assume that $\boldsymbol{\varepsilon}$ remains uniaxial, $\boldsymbol{\varepsilon} = \boldsymbol{\varepsilon}^{u}$, as in the N phase. Because $\mathbf{E}$ is parallel to the $\mathbf{Z}$ axis of the laboratory frame (Fig. 5, B and C), the electric term reads

$$\Delta f(E) = -\varepsilon_0 \mathbf{E}\cdot\boldsymbol{\varepsilon}^{u}\cdot\mathbf{E}/2 = -\varepsilon_0 \varepsilon^{u}_{ZZ} E^2/2 \quad (6)$$

As in the absence of the field, we obtain after energy minimization [see (*32*) and the Supplementary Materials]

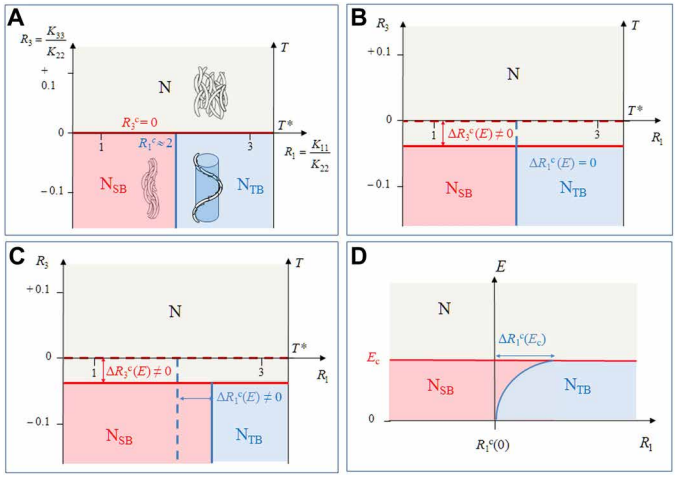


**Fig. 6. N-$N_{TB}$-$N_{SB}$ phase diagram in the presence of a field.** The phase diagram is represented as function of the ratios $R_1$ and $R_3(T)$ of the elastic constants (A to C) and as a function of the field $E$ and the ratio $R_1$ at a fixed temperature $T$ (D). (**A**) At $E = 0$, the N-MN second-order phase transition takes place at $R_3^c(T) = 0$, i.e., at $T = T^*$ and $K_{33} = 0$. The first-order $N_{TB}$-$N_{SB}$ transition is temperature independent and occurs at $R_1^c \approx 2$. (**B**) In the presence of a field and if the biaxiality of the MN phases is not taken into account, the N-MN transition is shifted to lower temperature by a field-dependent value. The $N_{TB}$-$N_{SB}$ transition remains field independent and again takes place at $R_1^c \approx 2$. (**C**) When the biaxiality of the MN phases is taken into account, the $N_{TB}$-$N_{SB}$ transition is shifted to higher $K_{11}/K_{22}$ values, which are a function of the field and the biaxiality of the dielectric tensor in the MN phases. The shift of the N-MN phase transition remains the same as in the uniaxial case. (**D**) Phase diagram as a function of the field at a constant temperature $T < T^*$. Up to the critical field $E_c(T)$, the modulated phases remain stable. The biaxial dielectric coupling favors the $N_{SB}$, and the $N_{TB}$-$N_{SB}$ transition is shifted to higher $K_{11}/K_{22}$ values. The shift, $\Delta R_1^c(E) = R_1^c(E) - R_1^c(0)$, increases quadratically with the field.

$$\bar{f}^{u}_{NTB}(E) = \bar{f}^{u}_{N}(E) + \frac{{K_{33}}^3}{108\,CK_{22}}[1 + r(E)][2 - r(E)]^2$$
$$\bar{f}^{u}_{NSB}(E) = \bar{f}^{u}_{N}(E) + \frac{{K_{33}}^3}{54\,CK_{11}}[1 + r(E)][2 - r(E)]^2 \quad (7)$$
$$\bar{f}^{u}_{N}(E) = -\frac{1}{2}\varepsilon_0 \varepsilon^{u}_{ZZ} E^2; \quad r(E) = \sqrt{1 + 12\,\varepsilon_0 \Delta\varepsilon^{u} E^2 \frac{C}{{K_{33}}^2}}$$

From these expressions, we obtain two field-induced N-$N_{TB}$ and N-$N_{SB}$ transitions, with the same field threshold, $E_{NTB-N} = E_{NSB-N} = \sqrt{\frac{K_{33}^2}{4\varepsilon_0 \Delta\varepsilon^{u} C}}$, and therefore the same field-induced shift of the transition temperature, $\Delta T_{NTB-N} = \Delta T_{NSB-N}$. At both of these N-MN field-induced transitions, the amplitude of the modulation, $\theta$ or $\theta_0$, respectively, is continuous (see fig. S4). Note that the modulation amplitude is a natural order parameter of the transition (it is finite in the "ordered" phase and zero in the "disordered" phase), and its continuity indicates that the transition is second order. In contrast, the wave number, $q$, jumps at the transition from its large finite value in the MN phase to an undefined value in the N phase (in the absence of a modulation wave, the wave number has no physical meaning).

The N-$N_{TB}$-$N_{SB}$ phase diagram for uniaxial coupling with the field (Fig. 6B) is very similar to that obtained at $E = 0$. The $N_{TB}$-$N_{SB}$ transition still occurs at $R_1^c(E) = R_1^c(0) = 2$, which shows that the observed field-induced $N_{TB}$-$N_{SB}$ transition cannot occur when the

dielectric tensor is uniaxial. The only field effect on the phase diagram is the shift of the MN-N transition by $\Delta R_3^c(E) = R_3^c(E) - R_3^c(0) = -2E\sqrt{\varepsilon_0 \Delta\varepsilon^u C}/K_{22}$, which corresponds to a small decrease of the N-MN transition temperature by $\Delta T^*(E) = -2E\sqrt{\varepsilon_0 \Delta\varepsilon^u K_{22}}\frac{\theta_{tb}}{a q_{tb}}$. This shift can be estimated from the constants of CB7CB close to the $N_{TB}$-N transition, which are already known from previous studies. With $E = 8$ V/μm, $\theta_{tb} \approx 0.2$ rad (*21*), $p_{tb} = \frac{2\pi}{q_{tb}} \approx 8$ nm (*16*, *18*, *19*), $\Delta\varepsilon^u \approx 2$ (*25*, *43*), $K_{22} \approx 8$ pN (*25*), and $a \approx 0.066$ pN/K [estimated by extrapolating the linear part of $K_{33}(T)$ in the N phase, see fig. S3], we obtain $\Delta T^*(E) \approx 0.7$°C. This value is larger than the observed shift, ≤0.2°C, which shows that the model overestimates the effect of the field on the transition.

If we now consider the biaxiality of **ε**, proceeding as before, we obtain (see the Supplementary Materials)

$$\tilde{f}_N^b(E) = \tilde{f}_N^u(E) = -\frac{1}{2}\varepsilon_0 \varepsilon^u{}_{zz} E^2$$
$$\tilde{f}_{NTB}^b(E) = \tilde{f}_N^u(E) + \frac{{K_{33}}^3}{108 C \widetilde{K}_{22}(E)}[1 + r(E)][2 - r(E)]^2 \quad (8)$$
$$\tilde{f}_{NSB}^b(E) = \tilde{f}_N^u(E) + \frac{{K_{33}}^3}{54 C \widetilde{K}_{11}(E)}[1 + r(E)][2 - r(E)]^2$$

where $r(E)$ is again given by Eq. 7 and

$$\widetilde{K}_{22}(E) = K_{22} + \frac{1}{2}\varepsilon_0 E^2 \beta_2 \delta\varepsilon^b; \quad \widetilde{K}_{11}(E) = K_{11} - \frac{1}{2}\varepsilon_0 E^2 \beta_2 \delta\varepsilon^b \quad (9)$$

are the effective twist and splay moduli, which are renormalized by the biaxiality of the dielectric tensor. We note that $\widetilde{K}_{22}(E) > K_{22}$ and $\widetilde{K}_{11}(E) < K_{11}$ (as $\beta_2 \delta\varepsilon^b > 0$), i.e., the biaxial dielectric coupling favors the $N_{SB}$ phase with respect to the $N_{TB}$ one.

The phase diagram for the biaxial case is shown in Fig. 6C. Although the position of the N-MN transition line remains exactly the same as in the uniaxial case, the $N_{TB}$-$N_{SB}$ transition now occurs at $\widetilde{R}_1(E) = \widetilde{K}_{11}(E)/\widetilde{K}_{22}(E) = 2$. This corresponds to a field-dependent critical value, $R_1{}^c(E) = 2 + \frac{3\varepsilon_0 \beta_2 \delta\varepsilon^b}{2K_{22}}E^2$, shifted upward compared to the previous field-independent value for the uniaxial case, $R_1^c(E) = R_1^c(0) = 2$.

Last, Fig. 6D shows the phase diagram at fixed temperature, $T < T^*$, as a function of the field strength and $R_1$ ratio. The N phase is stable above the threshold field $E_{MN-N} = -\frac{K_{33}}{\sqrt{4\varepsilon_0 \Delta\varepsilon^u C}} = \frac{a(T^* - T)}{\sqrt{4\varepsilon_0 \Delta\varepsilon^u C}}$. Below this threshold, the stable solution is a modulated nematic, either $N_{SB}$ for $R_1 < R_1^c(E)$ or $N_{TB}$ otherwise.

## DISCUSSION AND CONCLUSIONS

Qualitatively, the biaxial coupling with the electric field provides a satisfactory explanation of the experimentally observed features: the small decrease of the N-MN transition temperature and the field-induced $N_{TB}$ to $N_{SB}$ phase transition. This emphasizes the important role of the biaxial order in both modulated nematic phases. In the $N_{TB}$ phase, the biaxial order is only "local," at a scale smaller than the pitch, as the macroscopic symmetry of the phase is uniaxial (*9*, *16*, *34*, *36*, *37*). Therefore, for properties, like the birefringence, that are defined at the macroscopic scale, the local biaxiality plays only a minor role (*21*). In contrast, for the field-induced $N_{TB}$ to $N_{SB}$ phase transition, the biaxial coupling with the field acts on the microscopic structure of the phase and is not macroscopically averaged. Moreover, the dielectric biaxiality of the MN phases in the director frame, $\varepsilon^b{}_{yy} - \varepsilon^b{}_{xx} = \beta_2 \delta\varepsilon^b \mathbf{b}^2$, is important because of the large values of $\beta_2$ and $\delta\varepsilon^b$. $\beta_2$ is large because of the efficient coupling between the bent shape of the dimer and the director bend, leading to the spontaneous bend, and $\delta\varepsilon^b$ is large because of the much larger polarizability of the molecule in the **yz** plane than along the **x** axis. Furthermore, although **ε** is almost the same in both MN phases in the director frame, its macroscopic average component along the field, $\langle\varepsilon^b{}_{ZZ}\rangle$, differs in the two phases because of the different orientations of $\mathbf{Q}^b$ with respect to the field.

This combination of geometrical structure and local biaxiality of the two MN phases explains our most marked and counterintuitive result: An electric field, **E**, applied parallel to the symmetry axis **N** of the macroscopically uniaxial $N_{TB}$ phase, induces a transition to the macroscopically biaxial $N_{SB}$ phase. This effect is closely related to the local biaxial symmetry of the nematic order in both $N_{TB}$ and $N_{SB}$ phases because of the alignment of the biaxial bent-shaped molecule in the strongly bent director field. If this biaxiality is neglected, then no $N_{TB}$-$N_{SB}$ phase transition is expected when **E** ∥ **N**. In contrast, the transition was previously predicted and also reported in a completely different geometry where the field was applied perpendicular to the macroscopic symmetry axis, **E** ⊥ **N** (*31*–*33*, *44*). However, the phase transition is then intuitively expected because the uniaxial symmetry of the system is actually broken by the field. Similarly, the usual surface anchoring anisotropy, with the zenithal anchoring much stronger than the azimuthal, also breaks the uniaxial macroscopic symmetry of the $N_{TB}$ phase and has been predicted to promote a transition to the $N_{SB}$ phase (*35*).

Quantitatively, though, the experimental behavior is not properly captured by the elastic instability (*5*) and the flexoelectric (*9*) theoretical models because they both predict values of $R_1^c(0)$ of approximately 2 for the $N_{TB}$-$N_{SB}$ phase transition in zero field. Because the typical $K_{11}/K_{22}$ ratio is between 1 and 2 for nematics, including bent-shaped mesogens, the $N_{SB}$ phase should be much more common than the $N_{TB}$ one. In stark contrast, no experimental observation of the $N_{SB}$ phase was reported so far, whereas the $N_{TB}$ phase has been observed in numerous compounds.

This discrepancy might be due to an approximation adopted in both models. The modulated nematic is considered as an extension of the usual nematic, with $S$ continuous at the transition ($S_N = S_{MN}$) and uniform ($\nabla S_{MN} = 0$), and with periodic modulation of **n**. This approximation may be adequate for the $N_{TB}$ phase due to its roto-translational symmetry (**Q** is unchanged by an arbitrary translation $\Delta Z$ along **h** and simultaneous rotation by $\Delta\varphi = \Delta Z/p$ around **h**, leading to $\nabla S_{NTB} = 0$ and uniform amplitude of the bend). However, in the $N_{SB}$ phase, the bend is not uniform but instead oscillates along the modulation axis, and $\nabla S_{NSB} \neq 0$. Then, $S$ should also oscillate, in phase with $\mathbf{b}^2(Z)$, $S_{NSB}(Z) = S_N + \delta S_{NSB}\mathbf{b}^2(Z)$, resulting in an additional energy and shifting the $N_{TB}$-$N_{SB}$ transition line to a lower value of $K_{11}/K_{22}$.

For CB7CB, we have observed a symmetry-breaking $N_{TB}$-$N_{SB}$ transition under a moderate electric field. The low-field threshold of the induced phase transition comes from the large biaxial anisotropy of the molecule, $\delta\varepsilon^b$, and the strong coupling between **b** and $P$ ($P = \beta_2 \mathbf{b}^2$) in the two modulated nematic phases. Moreover, the low threshold indicates that, in the absence of a field, the representative point of the $N_{TB}$ phase of CB7CB in the generic phase diagram must lie very close to the $N_{TB}$-$N_{SB}$ transition line. A small renormalization of $K_{11}$ and $K_{22}$ by the field is enough to induce the transition. All these ideas provide important clues for guiding future efforts

toward the synthesis of compounds presenting the elusive $N_{SB}$ phase in the absence of a field. Considering the important role of biaxiality in the $N_{TB}$-$N_{SB}$ energy balance, strongly biaxial molecules (e.g., dimers or bent-core molecules with highly biaxial rigid cores, parallel to the **23**-plane in the molecular frame of reference) are expected to promote the $N_{SB}$ phase.

Because of the well-known equivalence (*1*, *45*) between electric and magnetic field effects in liquid crystals, the $N_{TB}$-$N_{SB}$ transition can also be expected when a strong magnetic field is applied to the $N_{TB}$ phase of a dimer with strongly biaxial magnetic susceptibility tensor. A possible indication of this effect is the birefringence behavior (*30*) observed in CB7CB under a magnetic field $B$ of 25 T. In the field, the value of $\Delta n$ is higher and its temperature dependence, $\Delta n(T)$, is very small compared to the steeper $\Delta n(T)$ curve in the zero-field case [see figure 3A in (*30*)]. This behavior is similar to that observed in our electric field experiment and might be due [at least partially, because in (*30*) the stripe texture of the cell also influences $\Delta n(T)$] to a magnetic field–induced, uniaxial symmetry-breaking $N_{TB}$-$N_{SB}$ transition.

Our observation of an electric field–induced transition from the $N_{TB}$ to $N_{SB}$ nematic phase demonstrates the important role of the local biaxiality of the MN phases. From a macroscopic point of view, this transition is counterintuitive: An electric field applied parallel to the symmetry axis of the macroscopically uniaxial $N_{TB}$ phase induces a transition to the macroscopically biaxial $N_{SB}$ phase. Our simple model taking into account the local biaxial order in the modulated phases describes qualitatively this transition. However, further development of the model, based on the biaxial order and its coupling with the nematic order parameter, is needed to reach a more quantitative description of the N-$N_{TB}$-$N_{SB}$ phase diagram. Progress in this direction is required to help guide the search for the still elusive $N_{SB}$ phase.

The discovery of $N_{SB}$-forming compounds will be an important breakthrough in liquid crystal applications. Because of the biaxiality of the $N_{SB}$ phase (at all scales, from the molecular to the macroscopic ones), novel electro-optic effects are expected even in the usual liquid crystal cell geometry, i.e., in planar alignment with the field applied perpendicular to the plates. These effects would lead to low-threshold voltages and on and off response times substantially faster than those of the usual nematics. The $N_{SB}$ phase will also present important advantages compared to the smectic phases: easy surface alignment, good uniformity and mechanical stability of the textures, and self-healing of the defects that may appear under mechanical, thermal, or electric shocks.

## MATERIALS AND METHODS

### Liquid crystal material

The mesogen used in the present study is the classic $N_{TB}$-forming, bent-shaped, liquid crystal dimer, CB7CB. There are two main reasons for this choice: The first one is that CB7CB is the best-characterized $N_{TB}$ material and most of its physical properties and their temperature dependences are reported in the literature, which greatly helps the interpretation of our results. The second reason is that CB7CB is particularly suitable for optic and electro-optic studies of the $N_{TB}$ phase: It has relatively large dielectric anisotropy, $\Delta\varepsilon \sim 2$, which gives rise to a strong response to the applied field; it is stable, without any degradation or shift of the phase-transition temperatures even when submitted for several days to strong electric fields, $E > 10$ V/μm; and, last, it forms, in thin cells, large monochiral domains in the $N_{TB}$ phase (*16*, *21*), allowing precise measurement of the birefringence in these domains and also in the defect walls between them.

The CB7CB had been carefully prepared using the methods described by Cestari *et al.* (*14*) and Barnes *et al.* (*46*), while Jokisaari *et al.* (*47*) give more recent, subtle details. The identity of the low-temperature nematic phase is given by Cestari *et al.* (*14*) as an $N_{TB}$ nematic, with the transition temperatures, $T_{NTB\text{-}N}$ and $T_{N\text{-}I}$, found to be 376 K and 389 K, respectively. These phase transitions were found to be first order in keeping with the $N_{TB}$ and N phases having the same symmetries (*42*); the respective entropies of transition, $\Delta S/R$, are 0.34 and 0.31, respectively (*46*).

### Electro-optic cell and experiment

For our study, we need to apply a strong and uniform electric field parallel to the macroscopic symmetry axis, **N**, of an $N_{TB}$ single domain. In principle, a natural choice for this kind of experiment would be to use a thin sandwich cell, with surface alignment layers providing homeotropic alignment of the liquid crystal. In this geometry, an electric field, **E**, applied to the nematic phase using transparent electrodes on the inner surfaces of the cell would be parallel to the surface-imposed director orientation, **E** || **n**. In the $N_{TB}$ phase, the homeotropic surface alignment of the director, **n**, would favor the homeotropic alignment of the helix axis, resulting in **E** || **N**, as desired. Unfortunately, this simple and attractive geometry of the experiment cannot be used in our case because it remains impossible to align CB7CB homeotropically (as for almost all the other $N_{TB}$-forming bent-shaped dimers). Actually, all the usual surface treatments used to achieve homeotropic alignment of nematics give, in the N and $N_{TB}$ phases of CB7CB, a strong and inhomogeneous planar alignment of **n** and **N**, respectively. Even when a strong field ($E = 10$ V/μm) is applied, only the bulk of the sample is aligned homeotropically, while the texture remains markedly inhomogeneous in the vicinity of the surfaces.

To resolve this issue in our electro-optic experiment, we used a cell with homogeneous planar alignment and applied a strong in-plane electric field parallel to the macroscopic symmetry axis of a well-aligned $N_{TB}$ single domain. Commercial liquid crystal cells do not match these requirements. In the most common type of cells, the field is applied across the cell gap, i.e., perpendicular to the alignment direction of the nematic, thus breaking the macroscopic uniaxial symmetry of the phase. Even in-plane–switching (IPS) cells, in which an in-plane electric field is applied by using interdigitated electrodes on one of the plates, are not suitable for our purposes. In these cells, the field is very inhomogeneous, because of the small pitch of the electrode comb, and it is perpendicular to the alignment direction of the nematic so that the macroscopic uniaxial symmetry of the phase is again broken.

To overcome this issue, we prepared homemade cells with in-plane field applied parallel to the planar alignment of the director, **n**, in the nematic phase, and of the helix axis, **h**, in the $N_{TB}$ phase. The cell architecture is presented in Fig. 2A. The top substrate is a glass plate without electrodes; the bottom one is a glass plate with a low-resistivity transparent indium-tin oxide (ITO)–deposited layer. This layer was etched to form two parallel electrodes on the plate, separated by an inter-electrode distance, $L_e$, of 50 μm. The cell gap, $d$, of ≈6 μm, is defined by ball spacers placed at the corners of the substrates, i.e., far away from the inter-electrode region. Figure 2B shows schematically the electric field lines when a voltage $U$ is applied

across the electrodes. The electric field **E** is perpendicular to the electrode edges and, midway between the electrodes, it is approximately uniform and parallel to the substrates, with an amplitude $E \approx U/L_e$. On both sides of this region and close to the electrode borders, the direction and strength of the field vary rapidly because of edge effects.

Both substrates were covered with a cured and uniaxially rubbed polyvinyl alcohol (PVA) film to impose uniform, planar alignment of the nematic director parallel to the rubbing direction, **r**, which was set perpendicular to the electrode stripes. Therefore, in the nematic phase, the electric field in the region of interest is uniform and parallel to the director (**E** || **r**). In the $N_{TB}$ phase, the axis of the director cone, **N**, and the helix axis, **h**, are both expected (*34*) to orient parallel to **r**, and therefore to **E**, as required for our experiment.

After sealing the cells with a photopolymerizable glue (NOA 81, Norland), the liquid crystal was filled by capillarity into the cells at 120°C in the isotropic phase and then cooled to the nematic and the $N_{TB}$ phases for the birefringence measurements. The temperature of the cell, placed on a heating stage (HS400, Instec), was controlled with 30-mK accuracy using a temperature controller (STC200D, Instec). All of the observations made with polarizing optical microscopy were performed with two microscopes: a Leitz 12 PolS microscope equipped with a Sony XC-HR70 grayscale digital camera and a color Nikon D50 camera and a Leica 2500P. The birefringence measurements (see Fig. 2C) were performed on the stage of the Leica 2500P with a Berek tilting compensator and a highly sensitive photodetector system. The latter consists of a photomultiplier tube (PMT; H6780, Hamamatsu) and an optical system, which allows the precise measurement of the intensity of the transmitted light in a small rectangular window in the image plane. We typically used a 15 μm × 60 μm window with its long side parallel to the electrodes and placed in the middle of the 50-μm inter-electrode gap, where the applied field is uniform and parallel to the optic axis of the sample, **n** or **N,** in the nematic and $N_{TB}$ phase, respectively.

A first approximate measurement of the birefringence was made with the usual Berek compensator technique. The slow axes of the cell and of the compensator were oriented perpendicular to each other and at 45° with respect to the crossed polarizers. Then, the tilt angle of the compensator plate, 2*i*, was varied to achieve the best compensation of the phase shifts introduced by the cell and the compensator, providing the value of the optical retardation of the cell, $d\Delta n$. Although this classical technique is very direct and fast, it is not precise enough for our purposes, because of the typical error bars of 10 nm on $d\Delta n$. This low precision originates from the low sensitivity of the human eye in detecting the minimum of the transmitted light intensity at the compensation. To avoid this issue, we measured the transmitted intensity from the voltage drop of the PMT anode current on a large load resistance (1 megohm), which was actually the input resistance of a digital oscilloscope (DPO3014, Tektronix) used to average the signal using up to 512 acquisitions. In this way, we measured the transmitted intensity as a function of the compensator tilt angle, $I(2i)$ (see Fig. 2D), and the parabolic fit of this function provides very precisely its minimum, which decreases the error bars on the optical retardation to <0.5 nm.

The signal applied to the electrodes was typically a square or sinusoidal alternating current (AC) waveform with a frequency in the range of 10 to 40 kHz. This signal was produced by an arbitrary waveform generator (TGA12101, TTI) with an amplitude $U \leq 10$ V and was then amplified by a wide-band amplifier (Krohn-Hite 7402 M) up to an amplitude of $U \leq 400$ V. This was the maximum voltage applied with a square waveform, resulting in a root mean square (RMS) in-plane field in the cell, $E_{RMS} \approx 8$ V/μm. When needed, higher RMS voltages, with a sinusoidal waveform, were applied with a homemade transformer, which further amplified the Krohn-Hite output voltage up to $U_{RMS} \approx 1000$ V. In most of our experiments, we used a cell, with $d = 6.3$ μm, with an applied square waveform AC field of $E_{RMS} = 8$ V/μm.

## Dielectric susceptibility tensor

The biaxiality of the modulated nematic phases is described by the secondary order parameter *P*. In principle, it is possible to calculate the order parameters *S* and *P* from molecular field models (*14*, *39*–*41*). However, in practice, this task is very difficult for bent-shaped dimers like CB7CB, and here, we will apply a simpler approximate approach based on the symmetry of the phases. Taking into account the molecular structure of the CB7CB dimer, we expect that $P > 0$, i.e., that the dimer is preferentially oriented with its **2**-axis parallel to the ***y*** axis of the director frame. This optimizes the orientation of the highly anisotropic rigid parts of the two monomer units with respect to the curved director field. To a first approximation, in the vicinity of the N-MN phase transition, we can assume that *S* is continuous at the transition and neglect its weak temperature dependence (*21*). In contrast, $P = 0$ in the uniform nematic phase but has a finite value in the MN phases, resulting from the large spontaneous bend **b**. We can then consider *P* as a scalar function of the scalar $\mathbf{b}^2$ and develop it in a series, $P = P(\mathbf{b}^2) = \sum_{i=0}^{\infty} \beta_{2i} \mathbf{b}^{2i}$, where $\beta_{2i}$ are constants, whose temperature dependence is supposed to be weak and will be neglected. Taking into account that $\mathbf{b} = 0$ and $P = 0$ in the N phase, we have $\beta_0 = 0$. Moreover, close to the transition, $\mathbf{b}^2$ can be considered as a small parameter, and we can truncate the expansion, retaining only the first term, $P = \beta_2 \mathbf{b}^2$. This simple expression is expected to apply to both the $N_{TB}$ and $N_{SB}$ phases because their local structures, at a scale much smaller than the pitch, are similar (a nematic phase with strong spontaneous bend distortion). In that sense, these two phases can be considered in a first approximation as two different "macroscopic textures" of the same spontaneously modulated nematic phase.

In both the uniaxial and biaxial cases, the dielectric tensor is diagonal in the director frame and can be expressed as a function of the order parameter tensor, which is, respectively, uniaxial, $\mathbf{Q}^u$, or biaxial, $\mathbf{Q}^b$

$$\boldsymbol{\varepsilon}^u = \begin{pmatrix} \varepsilon^u_{xx} & 0 & 0 \\ 0 & \varepsilon^u_{yy} & 0 \\ 0 & 0 & \varepsilon^u_{zz} \end{pmatrix} = \bar{\varepsilon}\mathbf{I} + \delta\varepsilon^u \mathbf{Q}^u = \begin{pmatrix} \bar{\varepsilon} - \frac{1}{2}\delta\varepsilon^u S & 0 & 0 \\ 0 & \bar{\varepsilon} - \frac{1}{2}\delta\varepsilon^u S & 0 \\ 0 & 0 & \bar{\varepsilon} + \delta\varepsilon^u S \end{pmatrix},$$

$$\boldsymbol{\varepsilon}^b = \begin{pmatrix} \varepsilon^b_{xx} & 0 & 0 \\ 0 & \varepsilon^b_{yy} & 0 \\ 0 & 0 & \varepsilon^b_{zz} \end{pmatrix} = \bar{\varepsilon}\mathbf{I} + \delta\varepsilon^u \mathbf{Q}^u + \delta\varepsilon^b \frac{P}{2} \begin{pmatrix} -1 & 0 & 0 \\ 0 & 1 & 0 \\ 0 & 0 & 0 \end{pmatrix} =$$

$$= \begin{pmatrix} \bar{\varepsilon} - \frac{1}{2}(\delta\varepsilon^u S + \delta\varepsilon^b P) & 0 & 0 \\ 0 & \bar{\varepsilon} - \frac{1}{2}(\delta\varepsilon^u S - \delta\varepsilon^b P) & 0 \\ 0 & 0 & \bar{\varepsilon} + \delta\varepsilon^u S \end{pmatrix} \tag{10}$$

where **I** is the unit tensor and $\bar{\varepsilon}$, $\delta\varepsilon^u$, and $\delta\varepsilon^b$ are constants describing, respectively, the isotropic part of $\boldsymbol{\varepsilon}$ and its uniaxial and biaxial

anisotropy. These constants are related to the components of the dielectric tensor in the molecular frame, $\boldsymbol{\varepsilon}^{M}$

$$\boldsymbol{\varepsilon}^{M} = \begin{pmatrix} \varepsilon^{M}_{11} & 0 & 0 \\ 0 & \varepsilon^{M}_{22} & 0 \\ 0 & 0 & \varepsilon^{M}_{33} \end{pmatrix} \tag{11}$$

Taking into account that the dielectric tensor of the N or MN phase is a statistical average of the molecular tensor $\boldsymbol{\varepsilon}^{M}$, $\boldsymbol{\varepsilon} = \langle \boldsymbol{\varepsilon}^{M} \rangle$, and considering the particular cases of a completely disordered (isotropic, $S = 0$, $P = 0$) and perfectly ordered uniaxial (nematic, $S = 1$, $P = 0$) or biaxial (modulated nematic, $S = 1$, $P = 1$) phases, we obtain

$$\bar{\varepsilon} = \frac{1}{3} Tr\, \varepsilon^{M} = \frac{1}{3}(\varepsilon^{M}_{11} + \varepsilon^{M}_{22} + \varepsilon^{M}_{33}) = \frac{1}{3} Tr\, \varepsilon^{u} = \frac{1}{3} Tr\, \varepsilon^{b},$$
$$\delta\varepsilon^{u} = \frac{1}{3}(2\varepsilon^{M}_{33} - \varepsilon^{M}_{11} - \varepsilon^{M}_{22}) = 2\frac{\varepsilon^{u}_{zz} - \frac{1}{2}(\varepsilon^{u}_{xx} + \varepsilon^{u}_{yy})}{3S} = \frac{2(\varepsilon^{u}_{\parallel} - \varepsilon^{u}_{\perp})}{3S} = \frac{2\Delta\varepsilon^{u}}{3S},$$
$$\delta\varepsilon^{b} = \varepsilon^{M}_{22} - \varepsilon^{M}_{11} = (\varepsilon^{b}_{yy} - \varepsilon^{b}_{xx})/P \tag{12}$$

We note that $\bar{\varepsilon}$, $\delta\varepsilon^{u}$, and $S$ can be measured in the nematic phase, just above the N-MN transition, which reduces the unknown parameters to $\delta\varepsilon^{b}$ and $P$, which are related to the biaxiality of the bent-shaped molecule and the modulated nematic phase, respectively. Moreover, we expect that the polarizability of the bent-shaped dimer is much larger in the plane **23**, because of the highly anisotropic rigid cores, than along axis **1**. Because the main contribution to $\boldsymbol{\varepsilon}^{M}$ is due to the molecular polarizability, we expect $\varepsilon^{M}_{22} > \varepsilon^{M}_{11}$, i.e., $\delta\varepsilon^{b} > 0$.

During the review process of our manuscript, Tomczyk and Longa (*48*) published a theoretical model that considers the role of the biaxiality of the order parameter tensor in modulated nematic phases. Using a generalized mean-field model, they predicted two distinct $N_{TB}$ nematic phases, $N_{TB}$ (macroscopically uniaxial) and $N_{TB,B}$ (macroscopically biaxial), for bent-core molecules. Further development of the model of (*48*) to describe the phase behavior under applied fields may clarify further the complex phase behavior of the modulated nematic phases and their broken uniaxial symmetry.

## SUPPLEMENTARY MATERIALS

Supplementary material for this article is available at http://advances.sciencemag.org/cgi/content/full/6/36/eabb8212/DC1

## REFERENCES AND NOTES


1. P. G. de Gennes, J. Prost, *The Physics of Liquid Crystals* (Clarendon, 1994).
2. F. C. Frank, On the theory of liquid crystals. *Disc. Farad. Soc.* **25**, 19–28 (1958).
3. M. J. Freiser, Ordered states of a nematic liquid. *Rev. Lett.* **24**, 1041–1043 (1970).
4. R. B. Meyer, in *Molecular Fluids*, R. Balian, G. Weill, Eds. (Gordon and Breach, 1976), vol. XXV, pp. 273–373.
5. I. Dozov, On the spontaneous symmetry breaking in the mesophases of achiral banana-shaped molecules. *Europhys. Lett.* **56**, 247–253 (2001).
6. N. Chaturvedi, R. D. Kamien, Mechanisms to splay-bend nematic phases. *Phys. Rev. E* **100**, 022704 (2019).
7. A. Mertelj, L. Cmok, N. Sebastian, R. J. Mandle, R. R. Parker, A. C. Whitwood, J. W. Goodby, M. Copic, Splay nematic phase. *Phys. Rev. X* **8**, 041025 (2018).
8. R. J. Mandle, A. Mertelj, Orientational order in the splay nematic ground state. *Phys. Chem. Chem. Phys.* **21**, 18769–18772 (2019).
9. S. M. Shamid, S. Dhakal, J. V. Selinger, Statistical mechanics of bend flexoelectricity and the twist-bend phase in bent-core liquid crystals. *Phys. Rev. E* **87**, 052503 (2013).
10. V. Goertz, C. Southern, N. W. Roberts, H. F. Gleeson, J. W. Goodby, Unusual properties of a bent-core liquid-crystalline fluid. *Soft Matter* **5**, 463–471 (2009).
11. C. Prasang, A. C. Whitwood, D. W. Bruce, Spontaneous symmetry-breaking in halogen-bonded, bent-core liquid crystals: Observation of a chemically driven Iso-N-N* phase sequence. *Chem. Commun.* , 2137–2139 (2008).
12. V. P. Panov, M. Nagaraj, J. K. Vij, Y. P. Panarin, A. Kohlmeier, M. G. Tamba, R. A. Lewis, G. H. Mehl, Spontaneous periodic deformations in nonchiral planar-aligned bimesogens with a nematic-nematic transition and a negative elastic constant. *Phys. Rev. Lett.* **105**, 167801 (2010).
13. V. P. Panov, R. Balachandran, M. Nagaraj, J. K. Vij, M. G. Tamba, A. Kohlmeier, G. H. Mehl, Microsecond linear optical response in the unusual nematic phase of achiral bimesogens. *Appl. Phys. Lett.* **99**, 261903 (2011).
14. M. Cestari, S. Diez-Berart, D. A. Dunmur, A. Ferrarini, M. R. de la Fuente, D. J. B. Jackson, D. O. Lopez, G. R. Luckhurst, M. A. Perez-Jubindo, R. M. Richardson, J. Salud, B. A. Timimi, H. Zimmermann, Phase behavior and properties of the liquid-crystal dimer 1″,7″-bis(4-cyanobiphenyl-4′-yl) heptane: A twist-bend nematic liquid crystal. *Phys. Rev. E* **84**, 031704 (2011).
15. P. A. Henderson, C. T. Imrie, Methylene-linked liquid crystal dimers and the twist-bend nematic phase. *Liq. Cryst.* **38**, 1407–1414 (2011).
16. C. Meyer, G. R. Luckhurst, I. Dozov, Flexoelectrically driven electroclinic effect in the twist-bend nematic phase of achiral molecules with bent shapes. *Phys. Rev. Lett.* **111**, 067801 (2013).
17. C. Greco, G. R. Luckhurst, A. Ferrarini, Enantiotopic discrimination and director organization in the twist-bend nematic phase. *Phys. Chem. Chem. Phys.* **15**, 14961–14965 (2013).
18. V. Borshch, Y. K. Kim, J. Xiang, M. Gao, A. Jakli, V. P. Panov, J. K. Vij, C. T. Imrie, M. G. Tamba, G. H. Mehl, O. D. Lavrentovich, Nematic twist-bend phase with nanoscale modulation of molecular orientation. *Nat. Commun.* **4**, 2635 (2013).
19. D. Chen, J. H. Porada, J. B. Hooper, A. Klittnick, Y. Shen, M. R. Tuchband, E. Korblova, D. Bedrov, D. M. Walba, M. A. Glaser, J. E. Maclennan, N. A. Clark, Chiral heliconical ground state of nanoscale pitch in a nematic liquid crystal of achiral molecular dimers. *Proc. Natl. Acad. Sci. U.S.A.* **110**, 15931–15936 (2013).
20. C. Zhu, M. R. Tuchband, A. Young, M. Shuai, A. Scarbrough, D. M. Walba, J. E. Maclennan, C. Wang, A. Hexemer, N. A. Clark, Resonant carbon K-edge soft X-ray scattering from lattice-free heliconical molecular ordering: Soft dilative elasticity of the twist-bend liquid crystal phase. *Phys. Rev. Lett.* **116**, 147803 (2016).
21. C. Meyer, G. R. Luckhurst, I. Dozov, The temperature dependence of the heliconical tilt angle in the twist-bend nematic phase of the odd dimer CB7CB. *J. Mater. Chem. C* **3**, 318–328 (2015).
22. L. Beguin, J. W. Emsley, M. Lelli, A. Lesage, G. R. Luckhurst, B. A. Timimi, H. Zimmermann, The chirality of a twist-bend nematic phase Identified by NMR spectroscopy. *J. Phys. Chem. B* **116**, 7940–7951 (2012).
23. K. Adlem, M. Copic, G. R. Luckhurst, A. Mertelj, O. Parri, R. M. Richardson, B. D. Snow, B. A. Timimi, R. P. Tuffin, D. Wilkes, Chemically induced twist-bend nematic liquid crystals, liquid crystal dimers, and negative elastic constants. *Phys. Rev. E* **88**, 022503 (2013).
24. N. Sebastian, D. O. Lopez, B. Robles-Hernandez, M. R. de la Fuente, J. Salud, M. A. Perez-Jubindo, D. A. Dunmur, G. R. Luckhurst, D. J. B. Jackson, Dielectric, calorimetric and mesophase properties of 1″-(2′,4-difluorobiphenyl-4′-yloxy)-9″-(4-cyanobiphenyl-4′-yloxy) nonane: An odd liquid crystal dimer with a monotropic mesophase having the characteristics of a twist-bend nematic phase. *Phys. Chem. Chem. Phys.* **16**, 21391–21406 (2014).
25. C.-J. Yun, M. R. Vengatesan, J. K. Vij, J.-K. Song, Hierarchical elasticity of bimesogenic liquid crystals with twist-bend nematic phase. *Appl. Phys. Lett.* **106**, 173102 (2015).
26. Z. Lu, P. A. Henderson, B. J. A. Paterson, C. T. Imrie, Liquid crystal dimers and the twist-bend nematic phase. The preparation and characterisation of the α,ω-bis(4-cyanobiphenyl-4 '-yl) alkanedioates. *Liq. Cryst.* **41**, 471–483 (2014).
27. R. J. Mandle, J. W. Goodby, Does topology dictate the incidence of the twist-bend phase? Insights gained from novel unsymmetrical bimesogens. *Chem. A Eur. J.* **22**, 18456–18464 (2016).
28. T. Ivsic, U. Baumeister, I. Dokli, A. Mikleusevic, A. Lesac, Sensitivity of the N-TB phase formation to the molecular structure of imino-linked dimers. *Liq. Cryst.* **44**, 93–105 (2017).
29. D. A. Paterson, J. P. Abberley, W. T. Harrison, J. M. Storey, C. T. Imrie, Cyanobiphenyl-based liquid crystal dimers and the twist-bend nematic phase. *Liq. Cryst.* **44**, 127–146 (2017).
30. P. K. Challa, V. Borshch, O. Parri, C. T. Imrie, S. N. Sprunt, J. T. Gleeson, O. D. Lavrentovich, A. Jakli, Twist-bend nematic liquid crystals in high magnetic fields. *Phys. Rev. E* **89**, 060501 (2014).
31. G. Pajak, L. Longa, A. Chrzanowska, Nematic twist-bend phase in an external field. *Proc. Natl. Acad. Sci. U.S.A.* **115**, E10303–E10312 (2018).
32. C. Meyer, Nematic twist-bend phase under external constraints. *Liq. Cryst.* **43**, 2144–2162 (2016).
33. K. Merkel, A. Kocot, J. K. Vij, G. Shanker, Distortions in structures of the twist bend nematic phase of a bent-core liquid crystal by the electric field. *Phys. Rev. E* **98**, 022704 (2018).
34. I. Dozov, C. Meyer, Analogy between the twist-bend nematic and the smectic A phases and coarse-grained description of the macroscopic N-TB properties. *Liq. Cryst.* **44**, 4–23 (2017).

35. P. Karbowniczek, M. Ciesla, L. Longa, A. Chrzanowska, Structure formation in monolayers composed of hard bent-core molecules. *Liq. Cryst.* **44**, 254–272 (2017).
36. C. Meyer, I. Dozov, Local distortion energy and coarse-grained elasticity of the twist-bend nematic phase. *Soft Matter* **12**, 574–580 (2016).
37. Z. Parsouzi, S. M. Shamid, V. Borshch, P. K. Challa, A. R. Baldwin, M. G. Tamba, C. Welch, G. H. Mehl, J. T. Gleeson, A. Jakli, O. D. Lavrentovich, D. W. Allender, J. V. Selinger, S. Sprunt, Fluctuation modes of a twist-bend nematic liquid crystal. *Phys. Rev. X* **6**, 021041 (2016).
38. L. M. Blinov, *Structure and Properties of Liquid Crystals* (Springer, 2011).
39. S. Kaur, H. Liu, J. Addis, C. Greco, A. Ferrarini, V. Gortz, J. W. Goodby, H. F. Gleeson, The influence of structure on the elastic, optical and dielectric properties of nematic phases formed from bent-core molecules. *J. Mater. Chem. C* **1**, 6667–6676 (2013).
40. M. Cestari, E. Frezza, A. Ferrarini, G. R. Luckhurst, Crucial role of molecular curvature for the bend elastic and flexoelectric properties of liquid crystals: Mesogenic dimers as a case study. *J. Mater. Chem.* **21**, 12303–12308 (2011).
41. C. Greco, G. R. Luckhurst, A. Ferrarini, Molecular geometry, twist-bend nematic phase and unconventional elasticity: A generalised Maier-Saupe theory. *Soft Matter* **10**, 9318–9323 (2014).
42. D. O. Lopez, B. Robles-Hernandez, J. Salud, M. R. de la Fuente, N. Sebastian, S. Diez-Berart, X. Jaen, D. A. Dunmur, G. R. Luckhurst, Miscibility studies of two twist-bend nematic liquid crystal dimers with different average molecular curvatures. A comparison between experimental data and predictions of a Landau mean-field theory for the $N_{TB}$-N phase transition. *Phys. Chem. Chem. Phys.* **18**, 6955–6955 (2016).
43. G. Babakhanova, Z. Parsouzi, S. Paladugu, H. Wang, Y. A. Nastishin, S. V. Shiyanovskii, S. Sprunt, O. D. Lavrentovich, Elastic and viscous properties of the nematic dimer CB7CB. *Phys. Rev. E* **96**, 062704 (2017).
44. K. Merkel, A. Kocot, C. Welch, G. H. Mehl, Soft modes of the dielectric response in the twist–bend nematic phase and identification of the transition to a nematic splay bend phase in the CBC7CB dimer. *Phys. Chem. Chem. Phys.* **21**, 22839–22848 (2019).
45. D. Dunmur, K. Toriyama, in *Handbook of Liquid Crystals*, D. Demus, J. Goodby, G. W. Gray, H.-W. Spiess, V. Vill, Eds. (Wiley-VCH, 1998), vol. 1.
46. P. J. Barnes, A. G. Douglass, S. K. Heeks, G. R. Luckhurst, An enhanced odd-even effect of liquid-crystal dimers. Orientational order in the α,ω-bis(4′-cyanobiphenyl-4-yl)alkanes. *Liq. Cryst.* **13**, 603–613 (1993).
47. J. P. Jokisaari, G. R. Luckhurst, B. A. Timimi, J. Zhu, H. Zimmermann, Twist-bend nematic phase of the liquid crystal dimer CB7CB: Orientational order and conical angle determined by $^{129}$Xe and $^{2}$H NMR spectroscopy. *Liq. Cryst.* **42**, 708–721 (2015).
48. W. Tomczyk, L. Longa, Role of molecular bend angle and biaxiality in the stabilization of the twist-bend nematic phase. *Soft Matter* **16**, 4350–4357 (2020).


**Acknowledgments:** We are indebted to T. Lubensky for discussions. **Funding:** This work was supported by the Agence Nationale pour la Recherche ANR (France) through grant BESTNEMATICS, ANR-15-CE24-0012, and by the Université de Picardie Jules Verne, Amiens, France. **Author contributions:** C.B. and I.D. designed the in-plane field cells and performed the birefringence measurements as a function of temperature and applied field. C.M., G.R.L., and I.D. developed the theoretical model. P.D., I.D., and G.R.L. wrote the manuscript with an input from all coauthors. **Competing interests:** The authors declare that they have no competing interests. **Data and materials availability:** All data needed to evaluate the conclusions in the paper are present in the paper and/or in the Supplementary Materials. Additional data related to this paper may be requested from the authors.

Submitted 21 March 2020
Accepted 20 July 2020
Published 2 September 2020
10.1126/sciadv.abb8212

**Citation:** C. Meyer, C. Blanc, G. R. Luckhurst, P. Davidson, I. Dozov, Biaxiality-driven twist-bend to splay-bend nematic phase transition induced by an electric field. *Sci. Adv.* **6**, eabb8212 (2020).

# Biaxiality-driven twist-bend to splay-bend nematic phase transition induced by an electric field

Claire Meyer, Christophe Blanc, Geoffrey R. Luckhurst, Patrick Davidson and Ivan Dozov

*Sci Adv* **6** (36), eabb8212.
DOI: 10.1126/sciadv.abb8212